

## Relationship between the fractal dimension of orthopyroxene distribution and the temperature in mantle xenoliths

**COLLIN NKONO<sup>1\*</sup>, OLIVIER FÉMÉNIAS<sup>2</sup>, ANNICK LESNE<sup>3</sup>, JEAN-CLAUDE MERCIER<sup>4,5</sup>,  
FADIMATOU YAMGOUOT NGOUNOUNO<sup>6</sup> and DANIEL DEMAIFFE<sup>1</sup>**

<sup>1</sup>Laboratoire de Géochimie, DSTE (CP 160/02), Université Libre de Bruxelles (ULB), Brussels, Belgium

<sup>2</sup>Avnel Gold Mining Limited, London, UK

<sup>3</sup>CNRS UMR 7600 (LPTMC), Université Pierre et Marie Curie-Paris 6, Sorbonne Universités, Paris, France

<sup>4</sup>UMR CNRS 6250 (LIENSs), ILE, Université of La Rochelle, La Rochelle, France

<sup>5</sup>UMR CNRS 6112 (LPNG), Université of Nantes, Nantes, France

<sup>6</sup>Université de Ngaoundéré, Faculté des Sciences, Département des Sciences de la Terre, Ngaoundéré, Cameroon

As rock textures reflect the physical conditions and the mechanisms of formation of the rocks, new approaches are used for improving texture analyses, both qualitatively and quantitatively. Pioneer work has recently boosted interest in fractal analysis for quantifying and correlating patterns. Fractal-like patterns relate to a degree of multiscale organization, and fractal dimensions (FD) and their potential variations can be used to infer the physical conditions of rock formation at various scales of observation. Here, we characterize quantitatively the shape and distribution of orthopyroxene grains in ultramafic xenoliths in terms of FD and their relation with temperature of equilibration. Fractal analysis has been applied to several populations of mantle xenoliths: 7 xenoliths collected in the vicinity of Pico Santa Isabel on Bioko Island, an alkaline basaltic volcano in oceanic domain (Gulf of Guinea, Equatorial Atlantic), 9 samples from Sangilen, in the Agardag alkaline lamprophyre dyke (Russia), and 11 samples from Śnieżnik (Lutynia, Poland), in the continental domain. Fractal analysis has been conducted to characterize the degree of complexity of the petrographic textures: it is indeed known that large values of FD are associated to more complex textures. The correlation here observed between the orthopyroxene fractal dimension and the temperature of equilibration suggests that FD captures a significant textural feature directly related to the temperature (i.e. generated by a temperature-controlled process). The significant difference in the FD–T correlation observed for the continental and oceanic mantle domains suggests that the mechanical and rheological behaviour is distinct in the oceanic and continental lithospheres. These first promising results should be confirmed by analysing other mantle suites of rocks in different geodynamic settings. Copyright © 2015 John Wiley & Sons, Ltd.

Received 15 March 2014; accepted 18 March 2015

KEY WORDS fractal dimension; mantle xenoliths; orthopyroxene; temperature

### 1. INTRODUCTION

The texture of a rock is generally defined, qualitatively, on the basis of the size, the modal proportion, the shape and the distribution of its rock-forming minerals. Several methods have been proposed to quantitatively characterize textures, but most of these depend exclusively on the grain size distribution (crystal size distribution CSD; i.e. Higgins, 2006). Although textures in metamorphic rocks are strongly related to the P–T equilibrium conditions and to the rate of deformation, there is still no clear quantitative relationship that links the texture of a sample to its conditions of formation.

Mantle-derived rocks—collectively called peridotites (mainly lherzolites) or ultramafic rocks—are essentially composed of three main minerals, olivine, orthopyroxene and clinopyroxene (in order of decreasing modal abundances, i.e. vol%), and a much less abundant Al-rich mineral whose nature depends on the pressure: plagioclase is only stable at low pressure, spinel at intermediate pressure and garnet at high pressure. These rocks mainly occur (1) as xenoliths in alkali basalts (spinel-bearing peridotites) and kimberlites (garnet-bearing peridotites) and (2) as orogenic peridotite massifs, often called Alpine-type peridotites. The textures of spinel-bearing peridotites from alkali basalts derived from the subcontinental mantle in Western Europe and from the suboceanic mantle in Hawaii have been extensively studied by Mercier and Nicolas (1975). Xenoliths from kimberlites were initially described by Boyd and Nixon (1972). Nixon

\*Correspondence to: C. Nkono, Laboratoire de Géochimie, DSTE (CP 160/02), Université Libre de Bruxelles (ULB), 50, Avenue Roosevelt, 1050 Brussels, Belgium. E-mail: cnkono@ulb.ac.be

(1987), edited a comprehensive book on 'Mantle xenoliths'. In this study, we use the largely accepted textural classification of Mercier and Nicolas (1975) with some synonymous terms proposed by Harte (1977). Three representative textural groups were defined (transitional stages exist between these groups): (1) protogranular (=coarse, *sensu* Harte, 1977). This group was further subdivided in two subgroups by Lenoir *et al.* (2000), protogranular *sensu stricto* and coarse-granular, (2) porphyroclastic (commonly observed in Alpine-type peridotites) and (3) equigranular (=mosaic or granuloblastic, *sensu* Harte, 1977). A fourth, largely subsidiary, texture, called poikiloblastic has been defined; it has been called 'coarse poikilitic' by, Downes *et al.* (1992).

The use of fractal geometry in the analysis of multi-scale irregular features observed in natural objects/systems has recently become critical in quantifying patterns and correlating these patterns to underlying processes. For instance, fractal analysis has been conducted to characterize textures of mantle xenoliths (Armienti and Tarquini, 2002), pyroclasts (Kueppers *et al.*, 2006), carbonates (Bili and Storti, 2004) and magmatic crystals (Bindeman, 2005), as well as fault or lineament distribution (Pérez-Lopez and Paredes, 2005; Nkono, 2008; Nkono *et al.*, 2013). In this paper, our aim is to quantify the degree of complexity of the orthopyroxene grain shape and spatial distribution in terms of fractal dimension (FD) and its relation with the temperature of equilibration. Orthopyroxene (opx) was chosen because (i) it is the most abundant phase among those that have been used for the calculation of the temperature of equilibration of mantle xenoliths and (ii) it displays deformation textures like kinking and polygonization (Mercier, 1976, 1980, 1985; Carbonell, 2004).

The fractal analysis of the orthopyroxene distribution has been applied to three series of samples representative of common mantle xenoliths: (1) 7 samples collected in the vicinity of the Pico Santa Isabel volcano on Bioko Island (Equatorial Guinea); this alkaline volcano belongs to the oceanic sector of the Cameroon volcanic line (Déruelle *et al.*, 2007); (2) 9 xenoliths from the Sangilen district in the Agardag alkaline lamprophyre dyke (Russia); and (3) 11 samples from the Śnieżnik (Lutynia) province (Western Sudetes, Poland). These two latter occurrences belong to the Central European Volcanic Province (CEVP; Wilson and Downes, 1991).

This study investigates the distribution of the overall fractal dimension of dynamically recrystallized polycrystalline orthopyroxene grains in mantle xenoliths.

## 2. GEOLOGICAL SETTING AND PETROGRAPHY

### 2.1. Bioko Island xenoliths

Bioko Island, located in the Gulf of Guinea, equatorial Atlantic Ocean (Fig. 1a) is the largest islands of the Cameroon

Hot Line (CHL, Déruelle *et al.*, 2007). Lavas erupted on Pico Santa Isabel and in the North-West part of the island contain abundant fresh peridotite xenoliths. The xenoliths used in this study have been collected by B. Déruelle (Univ P. et M. Curie, Paris, France) from large blocks of lavas, some 3 km to the northeast of the Pico Santa Isabel. Only fresh xenoliths devoid of any evidence of pyrometamorphism and/or impregnation by the host basalt were considered for further analyses. These friable samples were impregnated with epoxy under vacuum and polished thin-sections were prepared for petrological and mineralogical investigations.

All the xenoliths are typically medium- to coarse-grained rocks with a protogranular (Mercier and Nicolas, 1975; Mercier, 1985) or coarse granular (Lenoir *et al.*, 2000) texture, similar to that commonly observed worldwide in most spinel-peridotites (samples BX 19 and BX 23, Fig. 1b). Some rare xenoliths display porphyroclastic texture with olivine and orthopyroxene porphyroclasts showing moderate deformation features such as tabular sub-grains, exsolution lamellae and curvilinear grain boundaries (sample BX 30, Fig. 1b). Granuloblastic and/or poikiloblastic textures were not observed. Triple-point junctions at 120° are present. No penetrative fabric (foliation or lineation) has been macroscopically observed in any of these xenoliths. Deformation features such as subgrain boundaries in orthopyroxene and olivine are common (sample BX 22, Fig. 1b), but these can be regarded mostly as the result of high-stress solid-state deformation immediately prior to mantle sampling by the host lava (e.g. Tracy, 1980). On the whole, the xenoliths are anhydrous spinel harzburgites (Fig. 1c). Garnet-bearing xenoliths have never been found on Bioko. Modal proportions of the major phases were determined by microscopic observation: olivine (42 to 83 vol.%), orthopyroxene (opx) (13 to 55 vol.%), clinopyroxene (cpx) (2 to 7 vol.%), with spinel less than 1%. The compositional range of the studied peridotites is quite large (Table 1), ranging from opx-enriched rocks to opx-depleted, cpx-enriched rocks, so that some samples are lherzolites according to the IUGS classification (Le Maitre, 2002).

### 2.2. Sangilen xenoliths

The Tuva–Mongolian microcontinent is one of the largest continental blocks accreted during the Neoproterozoic and Palaeozoic orogenies in Central Asia. The southwestern part of this block constitutes the Sangilen Plateau in Russia (Fig. 1a) (Vladimirov *et al.*, 2005). This plateau is intruded by ultramafic to felsic igneous rocks (Izokh *et al.*, 2001; Vladimirov *et al.*, 2005). One of the youngest igneous episodes (447–441 Myr) formed the Agardag alkaline lamprophyre dyke complex (Izokh *et al.*, 2001; Vladimirov *et al.*, 2005; Gibsher *et al.*, 2012). These lamprophyre dykes contain rare mantle xenoliths (Egorova *et al.*, 2006;

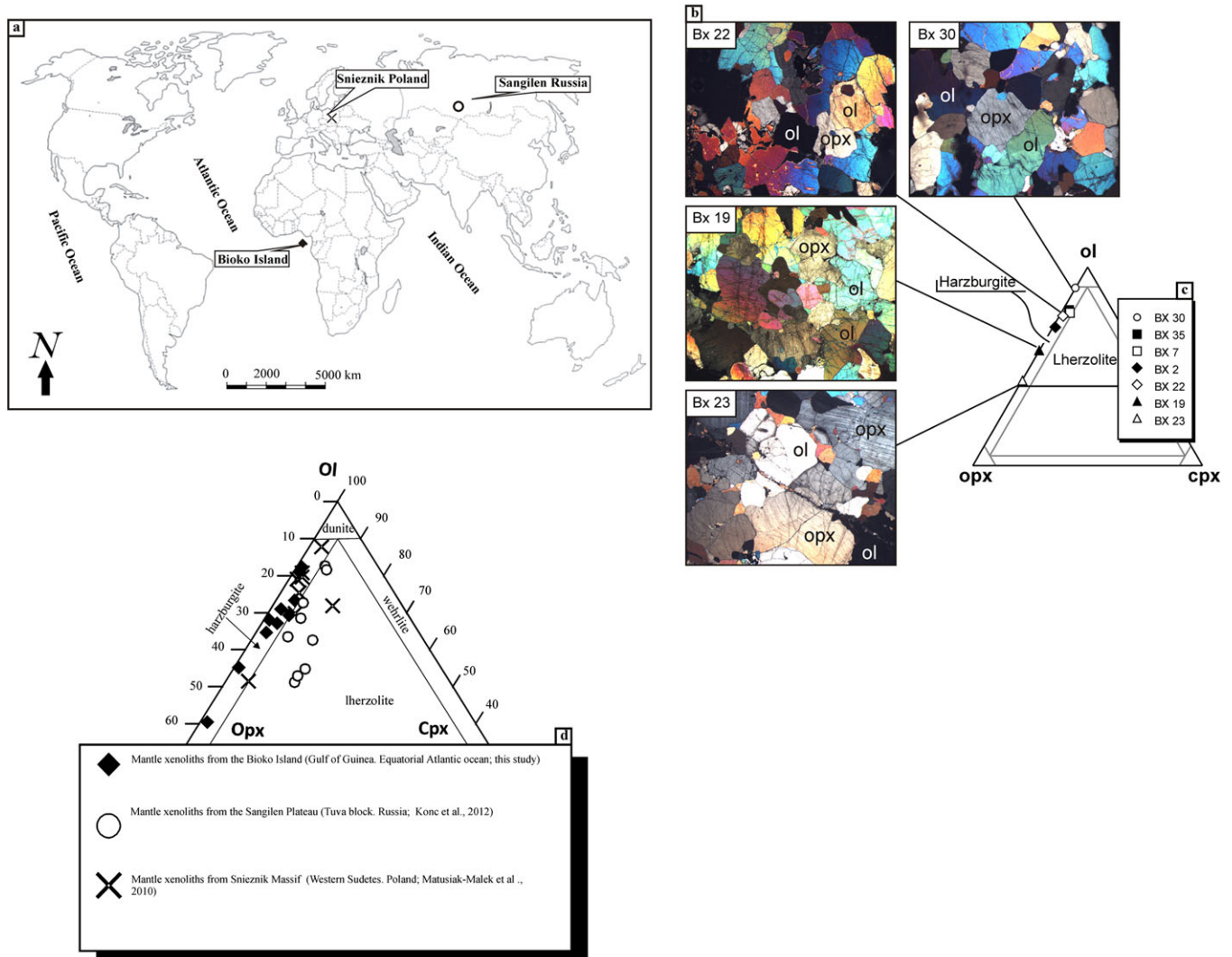


Figure 1. (a) General world map indicating the geographical location of the studied areas. (b) Photomicrographs of selected xenoliths from Pico Santa Isabel (Bioko Island) with typical petrographic textures: BX 22 and BX 30: porphyroclastic; BX 19: coarse granular; BX 23 coarse equigranular (Abbreviations: ol = olivine; opx = orthopyroxene; cpx = clinopyroxene); (c) IUGS classification of the ultramafic rocks (Le Maitre, 2002). (d) Plot of the modal compositions of the studied samples from the three areas in the IUGS classification diagram. This figure is available in colour online at [wileyonlinelibrary.com/journal/gj](http://wileyonlinelibrary.com/journal/gj)

Table 1. Mineral compositions (oxides in wt. %) and structural formulae for the main minerals (olivine, orthopyroxene, clinopyroxene) of the seven studied mantle xenoliths from Bioko Island. Temperature of equilibration ( $^{\circ}\text{C}$ ) based on the calibrations of Bertrand and Mercier (BM, 1985) and of Brey and Kohler (BK, 1990)

Olivine							
Samples	BX 2	BX 7	BX 19	BX 22	BX 23	BX 30	BX 35
SiO <sub>2</sub> (wt%)	41.15	41.49	41.40	41.21	41.46	41.42	40.95
Cr <sub>2</sub> O <sub>3</sub>						0.09	
FeO	9.61	8.48	8.61	8.54	8.85	8.50	9.12
MnO	0.12	0.16	0.12	0.13	0.26	0.14	0.11
MgO	48.93	49.31	49.29	48.89	49.39	49.92	49.26
CaO	0.10	0.09	0.09	0.07	0.06	0.08	0.06
Total	99.90	99.53	99.52	98.86	100.03	100.13	99.51

(Continues)

Table 1. (Continued)

<b>Olivine</b>							
Samples	BX 2	BX 7	BX 19	BX 22	BX 23	BX 30	BX 35
<i>Structural formula normalized on 4 O</i>							
Si	1.009	1.018	1.016	1.018	1.013	1.009	1.006
Cr						0.002	
Fe <sup>2+</sup>	0.197	0.174	0.177	0.176	0.181	0.173	0.187
Mn	0.002	0.003	0.003	0.003	0.005	0.003	0.002
Mg	1.789	1.803	1.803	1.800	1.799	1.812	1.803
Ca	0.002	0.002	0.002	0.002	0.002	0.002	0.001
Mg#	0.90	0.91	0.91	0.91	0.91	0.91	0.91
<b>Orthopyroxene</b>							
Samples	bx 2	bx 7	bx 19	bx 22	bx 23	bx 30	bx 35
SiO <sub>2</sub> (wt%)	56.19	56.20	56.07	55.76	56.14	57.33	55.68
Al <sub>2</sub> O <sub>3</sub>	2.84	3.22	2.91	3.23	3.07	1.52	3.01
Cr <sub>2</sub> O <sub>3</sub>	0.87	0.82	0.89	0.66	0.75	0.39	0.51
FeO	6.07	5.53	5.55	5.73	5.92	5.23	6.22
MnO		0.15	0.20	0.12			0.12
MgO	33.00	33.05	33.46	32.71	33.54	34.21	33.64
CaO	0.91	1.37	1.23	1.29	0.81	1.07	0.63
Na <sub>2</sub> O	0.08					0.06	0.04
Total	99.95	100.34	100.30	99.52	100.22	99.81	99.82
<i>Structural formula normalized on 6 O</i>							
Si	1.944	1.936	1.930	1.937	1.933	1.976	1.923
<sup>IV</sup> Al	0.056	0.064	0.070	0.063	0.067	0.024	0.077
<sup>VI</sup> Al	0.060	0.067	0.048	0.069	0.058	0.038	0.046
Cr	0.024	0.022	0.024	0.018	0.020	0.011	0.014
Fe <sup>2+</sup>	0.176	0.159	0.160	0.166	0.170	0.151	0.160
Mn		0.004	0.006	0.003			0.004
Mg	1.702	1.697	1.717	1.693	1.721	1.758	1.732
Ca	0.034	0.051	0.045	0.048	0.030	0.040	0.023
Na	0.006					0.004	0.002
Mg#	0.91	0.91	0.91	0.91	0.91	0.92	0.92
<b>Clinopyroxene</b>							
Samples	bx 2	bx 7	bx 19	bx 22	bx 23	bx 30	bx 35
SiO <sub>2</sub>	53.29	52.85	53.17	52.68	52.54	51.90	53.74
TiO <sub>2</sub>						0.55	0.06
Al <sub>2</sub> O <sub>3</sub>	2.85	3.37	3.02	3.44	3.74	4.71	2.98
Cr <sub>2</sub> O <sub>3</sub>	0.95	0.99	1.00	1.18	1.14	1.12	0.76
FeO	2.78	2.56	2.71	2.63	2.54	3.03	2.85
MnO		0.16					0.12
MgO	16.87	17.80	17.02	16.81	16.68	16.30	18.52
CaO	21.80	22.64	23.24	23.40	23.30	20.40	20.44
Na <sub>2</sub> O	0.59	0.05	0.23	0.19	0.21	1.08	0.61
Total	99.13	100.42	100.38	100.32	100.15	99.08	100.08
<i>Structural formula normalized on 6 O</i>							
Si	1.949	1.908	1.925	1.909	1.907	1.896	1.935
Ti						0.015	0.002
<sup>IV</sup> Al	0.051	0.092	0.075	0.091	0.093	0.104	0.065
<sup>VI</sup> Al	0.072	0.052	0.054	0.056	0.067	0.098	0.062
Fe <sup>3+</sup>	0.000	0.015	0.009	0.014	0.008	0.020	0.021
Fe <sup>2+</sup>	0.085	0.062	0.073	0.066	0.069	0.072	0.065
Mn		0.005					0.004

(Continues)

Table 1. (Continued)

Clinopyroxene							
Samples	bx 2	bx 7	bx 19	bx 22	bx 23	bx 30	bx 35
Mg	0.920	0.958	0.919	0.908	0.902	0.887	0.994
Ca	0.854	0.876	0.901	0.909	0.906	0.798	0.789
Na	0.042	0.004	0.016	0.013	0.015	0.076	0.043
Cr	0.027	0.028	0.028	0.034	0.033	0.032	0.022
Mg#	0.92	0.94	0.93	0.93	0.93	0.92	0.94
T BM °C	902	1015	830	1066	817	1212	1142
T BK °C	1004	1067	952	1075	934	1229	1164

Konc *et al.*, 2012) that were used in the present study and will be referred below as Sangilen xenoliths (Fig. 1c). The studied xenoliths, sampled from different localities of the Agardag alkaline lamprophyre dyke complex, are all spinel lherzolites. According to Konc *et al.* (2012) the Sangilen xenoliths display principally poikilitic (following Downes *et al.*, 1992) texture, less commonly coarse equigranular texture, and coarse granular (=protogranular) texture (Table 2).

### 2.3. Śnieżnik (Lutynia) xenoliths

Basaltic lavas, carrying mantle xenoliths, occur in the medium- to high-grade metamorphic Orlica–Śnieżnik dome (Western Sudetes Mts) in Poland (Fig. 1a). The basanites of Tertiary age (Birkenmajer *et al.*, 2002) belong to the Central European Volcanic Province (CEVP). The xenoliths from the ‘Szwedzkie Szańce’ quarry occur in a basaltic volcanic plug (Wierzchołowski, 1993) dated at  $4.56 \pm 0.2$  Ma (K–Ar age; Birkenmajer *et al.*, 2002). Most of the xenoliths are spinel harzburgites and spinel lherzolites (Fig. 1c and Table 2) displaying protogranular texture *sensu* Mercier and Nicolas (1975) and Matusiak-Małek *et al.* (2010).

## 3. MINERAL CHEMISTRY OF THE BIKO XENOLITHS

In this section, we present the chemical composition of the main minerals of the Bioko Island xenoliths. For the samples from other localities, the data are available in the papers of Matusiak-Małek *et al.* (2010) for Śnieżnik xenoliths and Konc *et al.* (2012) for the Sangilen xenoliths.

For Bioko samples, major element compositions of olivine, orthopyroxene, clinopyroxene and spinel have been determined by electron microprobe (CAMECA SX50) equipped with four wave length dispersive spectrometers (WDS) at the ‘Centre d’Analyses par Microsonde en Sciences de la Terre’ (CAMST), University of Louvain-la-Neuve, Belgium. The operating conditions involved an

accelerating voltage of 15 kV, a beam current of 20 nA and a counting time of 10 seconds for Fe, Mn, Ti, and Cr, 16 seconds for Si, Al, K and Mg, 24 seconds for Na. External calibrations were made with a combination of natural and synthetic mineral standards. The classical PAP correction was used.

The mineral compositions for the spinel-peridotites from Pico Santa Isabel (Table 1) are typical of Phanerozoic mantle. Olivine has a very restricted compositional range with Mg# {=molar Mg/(Mg+Fe)} varying from 0.90 to 0.91, which is similar to xenoliths worldwide (Frey and Prinz, 1978; Xu *et al.*, 1996, 1999; Ionov, 1998). Orthopyroxene is an enstatite with a narrow Mg# range (from 0.91 to 0.92). The Fe–Mg distribution between olivine and orthopyroxene suggests complete chemical equilibrium. Clinopyroxene is a diopside with Mg# varying from 0.92 to 0.93 and CaO and Al<sub>2</sub>O<sub>3</sub> contents varying from 20.40 to 23.63 wt.% and from 2.73 to 4.71 wt.% respectively (Table 1). Spinel displays quite large variations in Cr# (0.31 to 0.46) from sample to sample but is compositionally homogeneous at the thin-section scale. The Mg# of spinel ranges from 0.71 to 0.75 which is lower than for the other phases but is consistent with the spinel Fe–Cr intersite coupling.

## 4. DATA ACQUISITION AND PROCESSING

Mineral identification, grain-size automatic counting and texture analyses were performed on a combination of natural and cross-polarized light digital microphotographs. Images of the thin sections were acquired with a digital camera coupled with an optical polarizing microscope to get composite photographs of each section through an image editing software. The crystal boundaries have been extracted and/or redrawn through photo-processing softwares (Fig. 2a); the spatial regions occupied by orthopyroxene in a thin section have been delineated (Fig. 2b). The obtained digital images were used for fractal analysis of each sample.

Table 2. Fractal dimensions of the orthopyroxene ( $FD_{\text{opx}}$ ). Modal proportions of the main minerals in vol % (Ol: olivine; Opx: orthopyroxene; Cpx: clinopyroxene; Spl: spinel). Temperature of equilibration ( $^{\circ}\text{C}$ ) using the Brey and Kohler (BK) calibration (Brey and Kohler, 1990) for a fixed pressure of 1.5 GPa. Petrographic texture of the studied samples

Sample	$FD_{\text{Opx}}$	Olivine (%)	Opx (%)	Cpx (%)	spin (%)	T BK $^{\circ}\text{C}$	Texture
Mantle xenoliths from Xinhang area, SE China (after Liu <i>et al.</i> , 2012)							
<b>1</b>	1.554					900	Equigranular
<b>2</b>	1.422					1100	Coarse equigranular
<b>3</b>	1.30					800	Poikilitic**
<b>4</b>	1.05					900	Porphyroclastic
Mantle xenoliths from Bioko Island, Equatorial Africa (this study)							
<b>BX 2</b>	1.72	63.32	26.41	1.32	0.66	1004	Coarse granular*
<b>BX 7</b>	1.63	67.26	17.03	3.44	1.72	1067	Coarse granular*
<b>BX 19</b>	1.77	54.36	39.57	0.47	0.295	952	Coarse granular*
<b>BX 22</b>	1.70	69.8	21.36	2.52	1.635	1075	Porphyroclastic
<b>BX 23</b>	1.79	53.56	39.56	0.87	0.485	933	Coarse equigranular
<b>BX 30</b>	1.60	66.89	24.33	0.41	0.325	1229	Porphyroclastic
<b>BX 35</b>	1.64	65.98	25.15	2.53	1.265	1163	Equigranular
Mantle xenoliths from the NE Bohemian massif, Lutynia, SW Poland (after Matusiak-Matek <i>et al.</i> , 2010)							
<b>MM21</b>	1.73	87.67	8.93	2.37	1.03	995	
<b>MM39</b>	1.62	78.84	16.31	2	2.85	965	
<b>MM03</b>	1.71	51.6	38.91	5.01	4.48	985	
<b>MM08</b>	1.68	71.97	13.26	12.87	1.9	985	
<b>MM31</b>	1.67	69.71	21.77	6	2.52	957	
<b>MM25</b>	1.65	75.29	18.37	4.03	2.31	995	Protogranular
<b>MM28</b>	1.69	80.53	16.07	1.74	1.66	983	
<b>MM04</b>	1.61	80.27	16.12	2.02	1.59	1000	
<b>MM11</b>	1.64	75.56	16.01	6.62	1.81	955	
<b>MM22</b>	1.68	62.34	33.44	2.73	1.49	1000	
<b>MM09</b>	1.69	68.05	20.37	10.27	1.32	970	
Mantle xenoliths from Sangilen Plateau, Tuva, Southern Siberia, Russia (after Konc <i>et al.</i> , 2012)							
<b>3H-2</b>	1.71	63.4	26.5	7.6	2.5	1075	Coarse granular*
<b>3H-4</b>	1.8	51.1	32.7	15.2	1	1060	Poikilitic**
<b>3H-8</b>	1.67	52.8	31.9	15	0.3	1047	Poikilitic**
<b>5H-2</b>	1.66	54.7	29.1	15.7	0.5	1014	Coarse equigranular
<b>5H-3</b>	1.72	62.5	20.1	13.4	1.1	1083	Poikilitic**
<b>5H-7</b>	1.75	68.4	20.7	7.9	1.1	1021	Poikilitic**
<b>5H-9</b>	1.67	82.5	10.9	6.1	0.5	1062	Poikilitic**
<b>5H-10</b>	1.68	81.5	11.2	6.9	0.4	1047	Coarse
<b>5H-13</b>	1.69	72.6	20.9	6.3	0.2	1063	Poikilitic**

\*Coarse granular (Lenoir *et al.*, 2000) is a subgroup of the protogranular group of Mercier and Nicolas (1975).

\*\*Poikilitic (Downes *et al.*, 1992) = poikiloblastic of Mercier and Nicolas (1975).

#### 4.1. Fractal dimension analysis

A fractal distribution is essentially a self-similar distribution. Fractal distributions are used extensively in geology (e.g. Yielding *et al.*, 1992; Westaway, 1994; McCaffrey and Johnston, 1996) and in volcanology (e.g. Dellino and Liotino, 2002). Fractal analysis has been mainly used to statistically describe size or spatial frequency distributions (e.g. for faults), as well as for describing particle shapes (Jébrak, 1997). In general, the signature of the fractal nature of a particle or mass distribution is the relationship  $N(r) \sim r^{-D}$ , where  $r$  is a variable radius,  $N(r)$  is the number of particles or the mass contained in a ball of radius  $r$ , and  $D$  is the fractal dimension (FD). In our case, the texture of a given sample will be characterized by the fractal dimension of the distribution

of orthopyroxene grains in the thin section of this sample (Fig. 2b).

The FD (Fig. 2c) has been determined using the Fractalyse 2.4.1 software developed within the team 'City, mobility, territory' of ThéMA (Théoriser et Modéliser pour Aménager) of University of Franche-Comté in Bourgogne, France (Frankhauser *et al.*, 2007, 2008; Tarnier *et al.*, 2008a, 2008b). This software, originally developed for estimating the fractal dimension of the built area of cities (in our case, the 'built area' corresponds to the opx grains), can also be used to calculate the fractal dimension of a curve or a fault network. It proposes a dual option for performing a fractal analysis of an image or set of data: (1) vary the observation window  $r$  at a fixed resolution  $\varepsilon$  (pixel size), and

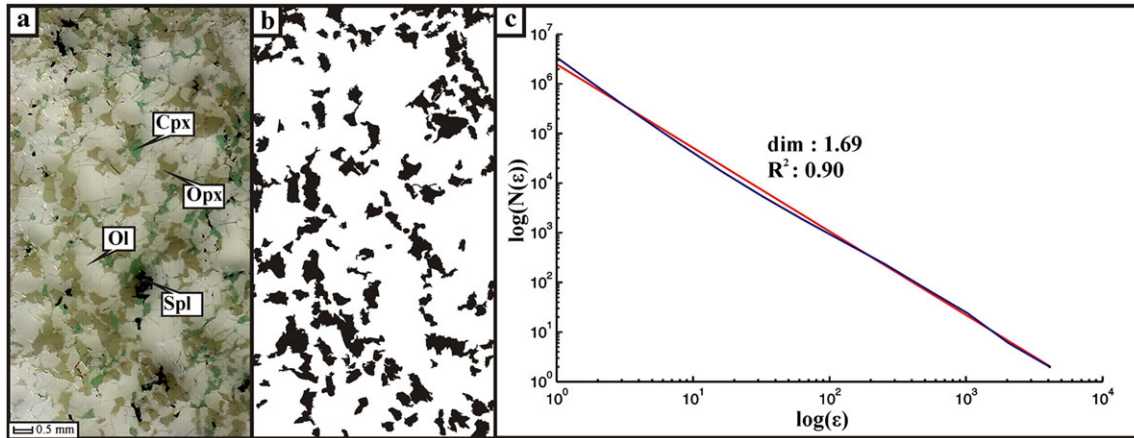


Figure 2. Data processing. (a) Microphotograph of a peridotite thin section. (b) 2D distribution (in black) of orthopyroxene drawn from this thin section. (c) Fractal Dimension (FD) computed at fixed observation window, by varying the resolution (apparent pixel size)  $\epsilon$ , and counting the number  $N(\epsilon)$  of  $\epsilon$ -pixels occupied by the orthopyroxene structure limited by the observation window. The red line represents the theoretical line; the blue line corresponds to the sample analysis. This figure is available in colour online at [wileyonlinelibrary.com/journal/gj](http://wileyonlinelibrary.com/journal/gj)

count the number  $N(r) \sim r^D$  of black pixels; the log–log plot of  $N(r)$  vs  $r$  would then display straight line of slope  $D$ . (2) fix the observation window (fixed size  $r$ ), vary the resolution (apparent pixel size)  $\epsilon$ , and count the number  $N(\epsilon) \sim \epsilon^{-D}$  of  $\epsilon$ -pixels occupied by the structure limited by the observation window (grid method) or the number  $N(\epsilon)$  of  $\epsilon$ -pixels required to cover the black structure (box counting method); the log–log plot of  $N(\epsilon)$  vs  $\epsilon$  would then display a straight line of opposite slope  $-D$ . The difference between the FD values obtained by the two methods (1) and (2) lies between 0.01 and 0.05, which is very small, so in this paper we consider only the values derived by applying the second calculation option (Fig. 2c).

Because a rock texture (or the photomicrograph of a thin section) is not a pure fractal (it is not a continuous structure but a discrete one spanning a finite range of scales), it is only possible to get an approximate fractal law, that is, the log–log plot of  $N(\epsilon)$  vs  $\epsilon$  displays only a roughly straight region, moreover in a finite range of scales. The slope value  $D$  is obtained from the best fit, its quality is appreciated by the correlation coefficient  $R$  (here  $R^2=0.90$ , Fig. 2c). For more information on the mathematical basis of the method, see the original papers of the Th MA laboratory (Frankhauser *et al.*, 2007, 2008; Tarnier *et al.*, 2008a, 2008b).

#### 4.2. Equilibrium temperatures

Equilibrium temperatures of mantle rocks can be estimated through many published geothermometers, each one having its own set of limitations but none having a particular universal application or support (Aldanmaz *et al.*, 2005). We use the geothermometer equations based on the pyroxene solvus models, with a pressure *a priori* fixed at 1.5 GPa. Two models were selected for comparison: the Bertrand and Mercier's

(1985) and the Brey and Kohler's (1990) formulations give very consistent  $T^\circ$  estimates (temperatures in  $^\circ\text{C}$ , respectively referred to as TBM and TBK) for Bioko samples (Fig. 3). To calculate the temperature, we used the compositions of clinopyroxenes and orthopyroxenes in both chemical and textural equilibrium. The 1.5 GPa pressure value has been chosen because it falls within the experimentally determined stability field of spinel-lherzolites (e.g. O'Neill, 1981). Moreover, it is commonly used in the literature, which allows straightforward comparisons with other studies.

For the xenoliths of  nieznik (Lutynia), Matusiak-Ma lek *et al.* (2010) calculated the temperatures using the opx–cpx geothermometers of Wells (1977) and Brey and Kohler

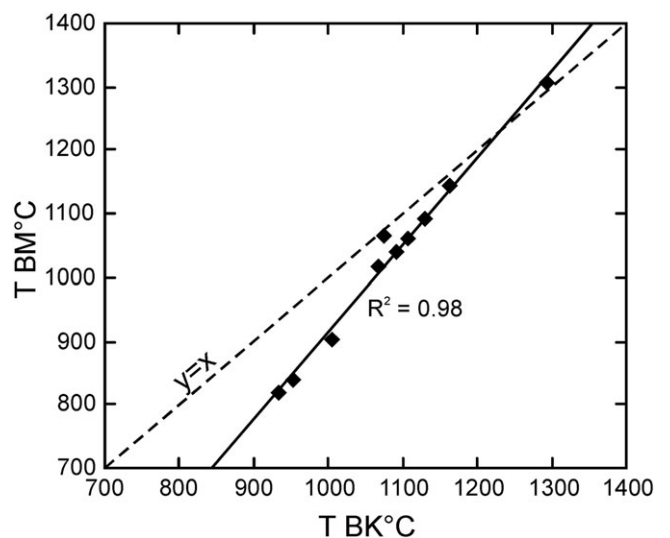


Figure 3. Correlation between the equilibrium temperatures estimated according to Bertrand and Mercier (1985) –  $T_{\text{BM}}^\circ\text{C}$ - and Brey and Kohler (1990) –  $T_{\text{BK}}^\circ\text{C}$ .

(1990) assuming a pressure of 1.5 GPa. For the Sangilen xenoliths, Konc *et al.* (2012) calculated equilibration temperatures using several geothermometric formulations for spinel peridotites:  $T_{\text{Cpx-Opx}}$ , two-pyroxene geothermometer of Taylor (1998);  $T_{\text{Ca-Opx}}$ , Ca-in orthopyroxene geothermometer of Brey and Kohler (1990);  $T_{\text{Ca-Opx-mod}}$ ,  $T_{\text{Ca-Opx}}$  formulation modified by Nimis and Grütter (2010); and  $T_{\text{Cr-Al-Opx}}$ , the Al-in-orthopyroxene geothermometer of Witt-Eickschen and Seck (1991).

To have a coherent set of  $T^\circ$  data, we use, for all samples, the common geothermometer of Brey and Kohler (1990).

## 5. RESULTS

### 5.1. Equilibrium temperature results

The equilibrium temperatures, for a fixed pressure of 1.5 GPa, obtained by using the mineral major element composition and the Brey and Köhler thermometer are reported in Table 1 for Bioko mantle xenoliths. The temperature of equilibration for the xenoliths from Bioko Island ranges from 933 °C to 1163 °C (Fig. 3). The Sangilen xenoliths were equilibrated between 1021 °C and 1083 °C and those of Śnieżnik (Lutynia) between 955 °C and 1000 °C (Table 2). These temperatures are interpreted as being representative of the true equilibrium temperatures of the spinel peridotites.

### 5.2. Fractal dimension results

We have defined above a fractal dimension that expresses the complexity of the overall properties of a texture. Twenty six microphotographs of thin sections from mantle xenoliths were analysed: 7 samples from Pico Santa Isabel on Bioko Island (Gulf of Guinea, equatorial Atlantic Ocean), 9 samples from Sangilen xenoliths collected in the Agardag alkaline lamprophyre dyke (Russia) and 11 samples collected in basanite lavas from Śnieżnik (Lutynia) in the Western Sudetes Mountains (Poland).

All the samples were analysed by the same method. The fractal dimension (FD) of the orthopyroxene spatial distribution (in thin sections) was obtained using the Fractalyse 2.4.1; the values are reported in Table 2. The ranges of FD for orthopyroxene in the different xenolith populations are: 1.60 to 1.79 for Bioko, 1.66 to 1.80 for Sangilen and 1.61 to 1.73 for Śnieżnik (Table 2). All analysed samples have FD values less than 2 which means that the orthopyroxene shape is effectively a fractal (a dense, homogeneous distribution of opx in the sample would have an integer dimension of 2). The large extent of the linear region in the log–log plot demonstrates that the distribution is statistically scale invariant over the range of thin section and the available spatial resolutions, and that measuring a FD makes sense.

## 6. DISCUSSION

Since all the studied xenoliths are spinel facies peridotites, calculation of their pressure of equilibration is difficult due to the lack of reliable geobarometers. Spinel is stable between 0.9 (Presnall *et al.*, 2002 and references therein) and 1.5 GPa (Klemme and O'Neill, 2000) at 1000 °C. By contrast, temperature can be easily estimated mainly by the two pyroxene geothermometers (see above). The P–T conditions alone can not directly be related to the textures of the xenoliths. The fractal dimension of the orthopyroxene distribution could be a potential new parameter in that respect. Our data and their interpretation will necessarily be preliminary as there are, to our knowledge, no other published fractal analysis for upper mantle rocks.

Figure 4 is a schematic cartoon illustrating the possible modification of the texture of a peridotite sample from its original solid state at depth in the mantle (position '1') to the left of the dry solidus of the peridotite to the deformed sub-surface (position '4') during its ascent through the lithosphere and its uptake as xenolith by a rising magma. The geotherm is constructed from equilibrium P–T conditions for garnet websterites (Xu *et al.*, 1999), for spinel peridotites (Sachtleben and Seck, 1981; Bertrand and Mercier, 1985; Xu *et al.*, 1996), the transition between spinel- and garnet-lherzolites is taken from O'Neill (1981). In this work we have characterized the complexity of the rock texture by the FD, more precisely by the FD of the orthopyroxene grain spatial distribution (in thin sections). To illustrate the variations of the textures in mantle rocks with depth, we have chosen four samples of Xianchan peridotites (Zhejiang province, S. China) from the detailed study of Liu *et al.* (2012). The samples are schematically illustrated by the cartoons '1' to '4' on Figure 4. It can be assumed that during the dynamic recrystallization of the minerals in the mantle, the growth rate and/or the deformation features are controlled not only by pressure and temperature but also, and probably mainly, by competition between the nucleation rate and grain-boundary-migration rate. Liu *et al.* (2012) have determined the P–T conditions of the peridotite xenoliths, which allows us to position them in the diagram. Moreover, they provided microphotographs of thin sections so that the FD of orthopyroxene can also be measured (Table 2). The FD increases with increasing texture complexity: it varies from 1.05 in sample '1' to 1.554 in sample '4'.

We have compared these results with those obtained on three mantle xenolith suites sampled in various geological environments, both in oceanic domain (Bioko Island, Gulf of Guinea) and continental domain (Sangilen plateau in Russia and Śnieżnik dome in Western Sudetes in Poland). The FD of the orthopyroxene in these xenoliths was used to infer the texture change. In all the studied samples, the

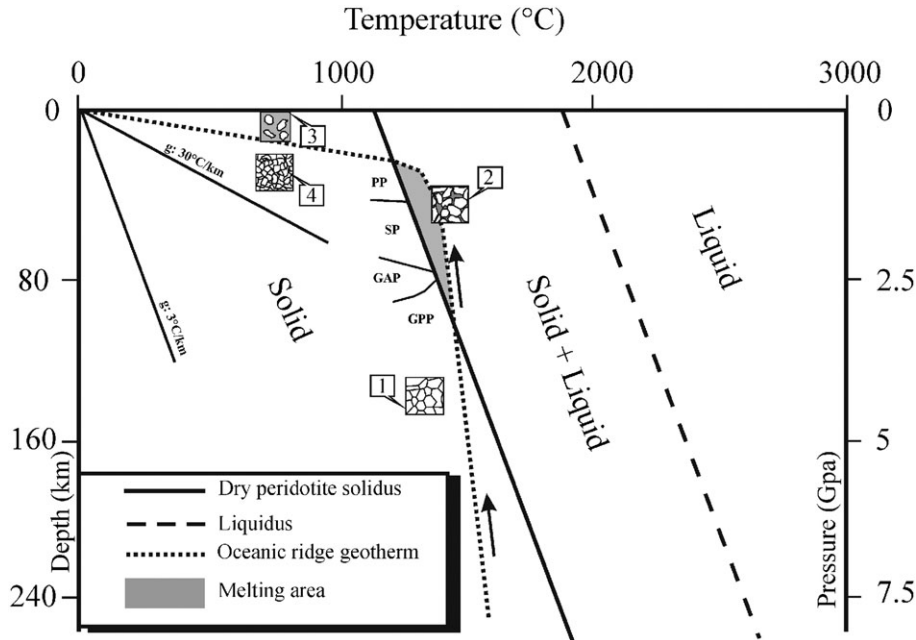


Figure 4. P–T diagram. Geotherms constructed from equilibrium P–T conditions for garnet websterites (calculated by different geothermobarometers; modified after Xu *et al.*, 1999). The equilibrium temperatures of spinel peridotites were determined by the thermometer of Sachtleben and Seck (1981) and Xu *et al.* (1996). The P–T range for spinel peridotites is constrained by the spinel–garnet transition and the equilibrium temperatures are estimated from the thermometer of Bertrand and Mercier (1985). The transition between spinel- and garnet-lherzolites is taken from O’Neill (1981). 1: Initial peridotite (minerals in the solid state) with equigranular/protogranular texture; 2: Partially melted peridotite with coarse equigranular texture; 3: Basaltic melt with glass, microliths and phenocrysts (poikilitic texture); 4: Residual peridotite with holocrystalline porphyroclastic texture. The photomicrographs and the P–T conditions for these samples are from Liu *et al.* (2012). PP: Plagioclase peridotite; SP: spinel peridotite; GAP: garnet peridotite; GPP: garnet and phlogopite peridotite.

orthopyroxene distribution follows the typical scale-invariant relation  $\{N(r) \sim r^D\}$  which is characteristic of a fractal structure. We can thus tentatively suggest that this type of grain distribution, namely the spatial distribution of the orthopyroxene crystals among the other minerals of the mantle xenoliths, seems to be a general feature of the upper mantle as a whole, whatever the geographical and/or geodynamic setting.

The results obtained for the seven samples from Bioko evidence a significant negative correlation (linear correlation with a negative slope) between the temperature of equilibration and the FD of the orthopyroxene (Fig. 5a). Qualitatively this type of correlation is consistent with the data obtained by Takahashi *et al.* (1998) and Takahashi and Nagahama (2001) who observed a decrease of the FD with increasing temperature for experimentally, dynamically recrystallized quartz grains, from 800 °C to 1000 °C. Samples from the two other localities (Sangilen and Śnieżnik) display an opposite relationship with an FD increase with increasing temperature (linear correlation with a positive slope, Fig. 5b), in other words with increasing depth.

The textural complexity of mantle xenoliths can be related to the deformation history of the rocks. We suggest that it could be estimated from the fractal dimension of the orthopyroxene grain distribution. In oceanic domain (Bioko

island), the rather thin, hot and young lithosphere (by comparison with the thicker and generally older and colder continental lithosphere) allows a fast ascent of the magmas and their xenoliths which therefore were not strongly deformed or recrystallized. This situation could explain the negative correlation between FD and temperature (Fig. 5a). By contrast, in continental domain (Sangilen and Śnieżnik) the thicker lithosphere presumably had, over time, a longer thermal and deformation history that induced complex textural reorganization, possibly responsible for the positive correlation between FD and T.

In their important paper on the thermal structure of the lithosphere, McKenzie *et al.* (2005) concluded ‘the mechanical behaviour of oceanic and continental upper mantle appears to depend on temperature alone and there is as yet no convincing evidence for compositional effect’ (p.317). They add ‘there is no convincing evidence that the rheology of continental and oceanic mantle is different’ (p.347). By contrast, our results show that the fractal dimension of orthopyroxene grain distribution in spinel-bearing upper mantle xenoliths is positively correlated with the temperature of equilibration in the continental domain and negatively correlated with temperature in the oceanic domain. If these FD measurements are effectively linked to the deformation and recrystallization history of the rocks, our

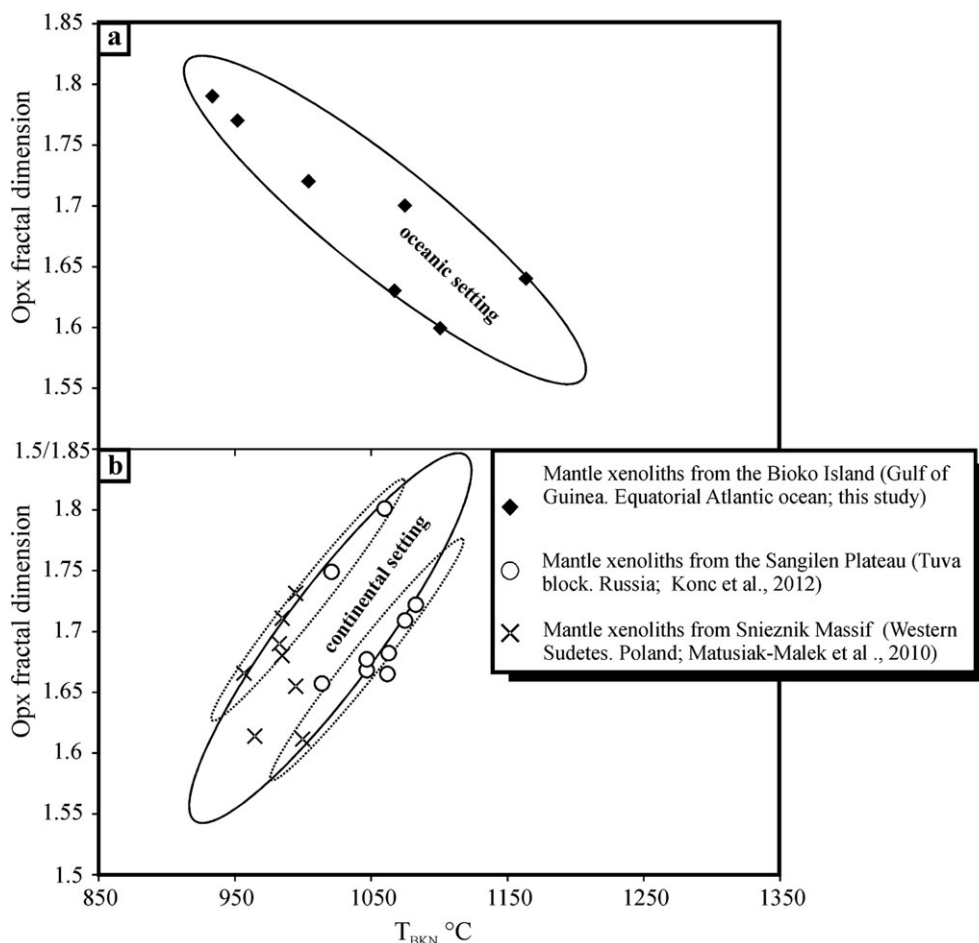


Figure 5. Correlation between the orthopyroxene fractal dimension (FD) and equilibrium temperature (calibration of Brey and Kohler, 1990). (a) Bioko island spinel peridotites (oceanic mantle). (b) Sangilen xenoliths (Russia) and the Śnieżnik (Poland) xenoliths (continental mantle).

experimental data on mantle rocks are in contradiction with the McKenzie *et al.* (2005) conclusions based on theoretical modelling of the lithosphere thermal structure. This contradiction is not really explained yet but McKenzie *et al.* (2005) stated that, in view of the uncertainty on the Moho temperature of shields, 'it is therefore still possible that the rheologies of oceanic and continental mantle are affected by composition as well as temperature' (p.347).

Although the data discussed in this paper are preliminary, they show: (1) correlations between the FD of orthopyroxene distribution in mantle xenoliths and their equilibrium temperature; such correlations were not recognized previously; (2) contrasting behaviours of oceanic and continental mantle domains in terms of mechanical and rheological properties.

The texture of the studied mantle xenoliths is characterized by the fractal dimension of their orthopyroxene grain distribution. Orthopyroxene is thus a mineral phase displaying a self-similar spatial distribution in these rocks. This texture could be the result of a still unidentified self-similar process such

as a critical thermodynamic state or a self-similar dynamic process. It thus appears that the present method for texture analysis—namely the determination of the fractal dimension of orthopyroxene grains—could bring new information besides the classical grain size counting and shape evaluation, especially for samples without clear foliation and with (optically) apparent similar grain size distribution.

Independent studies on other mantle suites of rocks are needed to confirm the preliminary conclusions of this paper and to shed some light on this interesting problem.

## 7. CONCLUSION

Rock textures are not easy to quantify. In this study, the fractal dimension (FD) of the orthopyroxene distribution in mantle xenoliths (essentially spinel-bearing harzburgites and lherzolites) has been measured in samples from three areas: (1) 7 samples from the Bioko Island (Gulf of Guinea,

equatorial Atlantic), (2) 9 samples from the Sangilen Plateau (Russia) and (3) 11 samples from Śnieżnik district (W Sudetes, Poland). The P–T equilibrium conditions were determined using available geothermometers, mainly the Brey and Kohler two-pyroxene thermometer.

The ranges of FD values are broadly similar for the three studied mantle suites: they are comprised between 1.60 and 1.80. FD and temperatures are negatively correlated for the oceanic Bioko mantle domain but positively correlated for the two other suites sampled in the continental domain. These contrasting results suggest that the rheological behaviour of the lithospheric mantle could be different in the oceanic and continental domains.

The good correlation observed between the fractal dimension of orthopyroxene distribution in mantle xenoliths and the temperature means that the FD captures a significant textural feature directly related to the temperature (i.e. generated by a temperature-controlled process). Our preliminary results could stimulate future research on the quantitative relationships between rock texture and the physical conditions of their formation.

#### ACKNOWLEDGEMENTS

We gratefully acknowledge the comments, suggestions and review of Dr Magdalena Matusiak-Malek. The authors also wish to thank Prof C. Moreau (Univ. de La Rochelle), and Prof P. Gaspard (ULB) for the discussions of many aspects of this work. CN was partly supported by a grant of the Van Buuren Foundation (ULB). Z. Konc, M. Matusiak-Malek, C.-Z. Liu, and S. Ayong are acknowledged for providing microphotographs of mantle xenoliths used in this work.

#### REFERENCES

- Aldanmaz, E., Köprübaşı, N., Gürer, Ö.F., Kaymakçı, N., Gourgaud, A. 2005. Geochemical constraints on the Cenozoic, OIB-type alkaline volcanic rocks of NW Turkey: implications for mantle sources and melting processes. *Lithos* **86**, 50–76.
- Armienti, P., Tarquini, S. 2002. Power law olivine crystal size distribution in lithospheric mantle xenoliths. *Lithos* **65**, 272–285.
- Bertrand, P., Mercier, J.-C. 1985. The mutual solubility of coexisting ortho- and clinopyroxene: toward an absolute geothermometer for natural system. *Earth and Planetary Science Letters* **76**, 109–122.
- Bili, A., Storti, F. 2004. Fractal distribution of particle size in carbonate cataclastic rocks from the core of a regional strike-slip fault zone. *Tectonophysics* **384**, 115–128.
- Bindeman, I.N. 2005. Fragmentation phenomena in populations of magmatic crystals. *American Mineralogist* **90**, 1801–1815.
- Birkenmajer, K., Pécskay, Z., Grabowski, J., Lorenc, M.W., Zagożdżon, P.P. 2002. Radiometric dating of the Tertiary volcanics in Lower Silesia, Poland. II. K–Ar and paleomagnetic data from Neogene basanites near Łądek Zdrój, Sudetes Mountains. *Annales. Societatis Geologorum Poloniae* **72**, 119–121.
- Boyd, F.R., Nixon, P.H. 1972. Ultramafic nodules from the Thaba Putsoa Kimberlite pipe. Carnegie Institute Washington. Annual Report of Director Geophysics, Laboratory. *Year Book* **81**, 362–373.
- Brey, G.P., Kohler, T. 1990. Geothermobarometry in four phase lherzolites II. New thermobarometers, and practical assessment of existing thermobarometers. *Journal of Petrology* **31**(6), 1353–1378.
- Carbonell, R. 2004. On the nature of mantle heterogeneities and discontinuities: evidence from a very dense wide-angle shot record. *Tectonophysics* **388**, 103–117.
- Dellino, P., Liotino, G. 2002. The fractal and multifractal dimension of volcanic ash particles contour: a test study on the utility and volcanological relevance. *Journal of Volcanological and Geothermal Research* **113**, 1–18.
- Déruelle, B., Ngounouno, I., Demaiffe, D. 2007. The “Cameroon hot line”: A unique example of active alkaline intraplate structure in both oceanic and continental lithosphere. *Comptes Rendus Geoscience* **339**, 589–600.
- Downes, H., Embey-Isztin, A., Thirlwall, M. 1992. Petrology and geochemistry of spinel-bearing peridotite xenoliths from the western Pannonian Basin (Hungary)/evidence for an association between enrichment and texture in upper mantle. *Contributions to Mineralogy and Petrology* **109**, 340–354.
- Egorova, V.V., Volkova, N.I., Shelepaev, R.A., Izokh, A.E. 2006. The lithosphere beneath the Sangilen Plateau, Siberia: evidence from peridotite, pyroxenite and gabbro xenoliths from alkaline basalts. *Mineralogy and Petrology* **88**, 419–441.
- Frankhauser, P., Tarnier, C., Vuidel, G., Houot, H. 2007. *Approche fractale de l'urbanisation, méthodes d'analyse, d'accessibilité et simulations multi-échelles*. 11th World Conference on Transportation Research, Geography, Berkeley, 21 pp.
- Frankhauser, P., Tarnier, C., Vuidel, G., Houot, H. 2008. *Une approche multi-échelle de l'accessibilité pour maîtriser l'étalement urbain*. Colloque mobil. TUM2008 à Munich, 19 pp.
- Frey, F.A., Prinz, M. 1978. Ultramafic inclusions from San Carlos, Arizona: petrological and geochemical data bearing on their petrogenesis. *Earth and Planetary Science Letters* **38**, 129–176.
- Gibsher, A.A., Malkovets, V.G., Travin, A.V., Belousova, E.A., Sharygin, V.V., Konc, Z. 2012. The age of camptonite dikes of the Agardag alkali-basalt complex (western Sangilen): results of Ar/Ar and U/Pb dating. *Russian Geology and Geophysics* **53**, 998–1013.
- Harte, B. 1977. Rock nomenclature with particular relation to deformation and recrystallization textures in olivine-bearing xenoliths. *Journal of Geology* **85**, 279–288.
- Higgins, M.D. 2006. Verification of ideal semi-logarithmic, lognormal or fractal crystal size distribution from 2D datasets. *Journal of Volcanology and Geothermal Research* **154**, 8–16.
- Ionov, D.A. 1998. Trace element composition of mantle-derived carbonates and coexisting phases in peridotite xenoliths from alkali basalts. *Journal of Petrology* **39**, 1931–1941.
- Izokh, A.E., Polyakov, G.V., Malkovets, V.G., Shelepaev, R.A., Travin, A.V., Litasov, Y.D., Gibsher, A.A. 2001. The Late Ordovician age of camptonites from the Agardag Complex of southeastern Tuva as an indicator of the plume-related magmatism during collision processes. *Doklady Earth Sciences* **379**, 511–514.
- Jébrak, M. 1997. Hydrothermal breccias in vein-type ore deposits: a review of mechanisms, morphology and size distribution. *Ore Geology Reviews* **12**, 111–134.
- Klemme, S., O'Neill, H.StC. 2000. The near-solidus transition from garnet lherzolite to spinel lherzolite. *Contributions to Mineralogy and Petrology* **138**, 237–248.
- Konc, Z., Marchesi, C., Hidas, K., Garrido, C.J., Szabó, C., Sharygin, V.V. 2012. Structure and composition of the subcontinental lithospheric mantle beneath the Sangilen Plateau (Tuva, southern Siberia, Russia): evidence from lamprophyre-hosted spinel peridotite xenoliths. *Lithos* **146–147**, 253–263.
- Kueppers, U., Scheu, B., Spieler, O., Dingwell, D.B. 2006. Fragmentation efficiency of explosive volcanic eruptions: a study of experimentally generated pyroclasts. *Journal of Volcanology and Geothermal Research* **153**, 125–135.
- Le Maitre, R.W. 2002. *Igneous Rocks. A Classification and Glossary of Terms. Recommendations of the International Union of Geological*

- Sciences Subcommittee on the Systematics of Igneous Rocks*, 2nd edn. Cambridge University Press: Cambridge, New York, Melbourne, 1–236.
- Lenoir, X., Garrido, C.J., Bodinier, J.L., Dautria, J.M. 2000.** Contrasting lithospheric mantle domains beneath the Massif Central (France) revealed by geochemistry of peridotite xenoliths. *Earth and Planetary Science Letters* **181**, 359–375.
- Liu, C.-Z., Wu, F.-Y., Sun, J., Chu, Z.-Y., Qiu, Z.-L. 2012.** The Xinchang peridotite xenoliths reveal mantle replacement and accretion in southeastern China. *Lithos* **150**, 171–187.
- Matusiak-Malek, M., Puziewicz, J., Ntafos, T., Grégoire, M., Downes, H. 2010.** Metasomatic effects in the lithospheric mantle beneath the NE Bohemian Massif: a case study of Lutynia (SW Poland) peridotite xenoliths. *Lithos* **117**, 49–60.
- McCaffrey, K.J.W., Johnston, J.D. 1996.** Fractal analysis of a mineralised vein deposit: Curraghinalt gold deposit, County Tyrone. *Mineralium Deposita* **31**, 52–58.
- McKenzie, D., Jackson, J., Priestley, K. 2005.** Thermal structure of oceanic and continental lithosphere. *Earth and Planetary Science Letters* **233**, 337–349.
- Mercier, J.-C.C. 1976.** Single-pyroxene geothermometry and geobarometry. *American Mineralogist* **61**, 603–615.
- Mercier, J.-C.C. 1980.** Magnitude of the lithospheric stresses inferred from rheomorphic petrology. U.S. National Earthquake hazards Reduction program. *Open-file Report* **625**, 771–802.
- Mercier, J.-C.C. 1985.** Olivine et pyroxènes. In: *Preferred Orientation in Deformed Metals and Rocks: an Introduction to Modern Texture Analysis*, R.W. Wenk (ed.). Chapter 19, Academic Press: New York; 407–430.
- Mercier, J.-C.C., Nicolas, A. 1975.** Textures and fabrics of upper-mantle peridotites as illustrated by xenoliths from basalts. *Journal of Petrology* **16**, 454–487.
- Nimis, P., Grütter, H. 2010.** Internally consistent geothermometers for garnet peridotites and pyroxenites. *Contributions to Mineralogy and Petrology* **159**, 411–427.
- Nixon, P.H. (ed.) 1987.** *Mantle Xenoliths*. J. Wiley & Sons: Chichester; 1–844.
- Nkono, C. 2008.** *Analyse multi-échelle et interprétation géodynamique des données morphostructurales associées au volcano-plutonisme phanérozoïque d'Afrique équatoriale (ligne du Cameroun et régions voisines)*. Ph.D Thesis, Université Libre de Bruxelles (ULB) 356 pp.
- Nkono, C., Féménias, O., Lesne, A., Mercier, J.-C.C., Demaiffe, D. 2013.** Fractal Analysis of lineaments in Equatorial Africa: insights on lithospheric structure. *Open Journal of Geology* **3**, 157–168.
- O'Neill, H.St.C. 1981.** The transition between spinel lherzolite and garnet lherzolite, and its use as geobarometer. *Contributions to Mineralogy and Petrology* **77**, 251–255.
- Pérez-Lopez, R., Paredes, C. 2005.** On measuring the fractal anisotropy of 2-D geometrical sets: application to the spatial distribution of fractures. *Geoderma* **134**, 402–414.
- Presnall, D.C., Gudfinnsson, G.H., Walter, M.J. 2002.** Generation of mid-ocean ridge basalts at pressures from 1 to 7 GPa. *Geochimica et Cosmochimica Acta* **66**, 2073–2090.
- Sachtleben, T., Seck, H.A. 1981.** Chemical control on the Al solubility in orthopyroxene and its implications on pyroxene geothermometry. *Contributions to Mineralogy and Petrology* **78**, 157–165.
- Takahashi, M., Nagahama, H. 2001.** The section' fractal dimension of grain boundary. *Applied Surface Sciences* **182**, 297–301.
- Takahashi, M., Nagahama, H., Masuda, T., Fujimura, A. 1998.** Fractal analysis of experimentally, dynamically recrystallized quartz grains and its possible application as a strain rate meter. *Journal of Structural Geology* **20**, 269–275.
- Tarnier, C., Vuidel, G., Frankhauser, P. 2008a.** *Délimitation d'ensembles morphologiques par une approche multi-échelle—application à la délimitation morphologique des agglomérations*. Huitièmes Rencontres de Théo Quant, Besançon, 14 pp.
- Tarnier, C., Vuidel, G., Frankhauser, P., Houot, H. 2008b.** *An urban multi-scale simulation tool using fuzzy evaluation of accessibility and morphological constraints*. 48th Congress of the European Regional Science Association, Liverpool.
- Taylor, W.R. 1998.** An experimental test of some geothermometer and geobarometer formulations for upper mantle peridotites with application to the thermobarometry of fertile lherzolite and garnet websterite. *Neues Jahrbuch Fur Mineralogie, Abhandlungen* **172**, 381–408.
- Tracy, R.T. 1980.** Petrology and genetic significance of an ultramafic xenolith suite from Tahiti. *Earth and Planetary Science Letters* **48**, 80–96.
- Vladimirov, V.G., Vladimirov, A.G., Gibsher, A.S., Travin, A.V., Rudnev, S.N., Shemelina, I.V., Barabash, N.V., Savinykh, Y.V. 2005.** Model of the tectonometamorphic evolution for the Sangilen block (South-eastern Tuva, Central Asia) as a reflection of the early Caledonian accretion–collision tectogenesis. *Doklady Earth Sciences* **405**, 1159–1165.
- Wells, P.R.A. 1977.** Pyroxene thermometry in simple and complex systems. *Contributions to Mineralogy and Petrology* **62**, 129–139.
- Westaway, R. 1994.** Quantitative analysis of populations of small faults. *Journal of Structural Geology* **16**, 1259–1273.
- Wierzbolowski, B. 1993.** Stanowisko systematyczne i geneza sudeckich skał wulkanicznych. *Archiwum Mineralogiczne* **49**, 199–235 (in Polish).
- Wilson, M., Downes, H. 1991.** Tertiary–Quaternary extension-related alkaline magmatism in Western and Central Europe. *Journal of Petrology* **32**, 811–849.
- Witt-Eickchen, G., Seck, H.A. 1991.** Solubility of Ca and Al in orthopyroxene from spinel peridotite—an improved version of an empirical geothermometer. *Contributions to Mineralogy and Petrology* **106**, 431–439.
- Xu, Y., Lin, C., Shi, L. 1999.** The geotherm of the lithosphere beneath Qilin, SE China: a re-appraisal and implications for P–T estimation of Fe-rich pyroxenites. *Lithos* **47**, 181–193.
- Xu, X.S., O'Reilly, S.Y., Zhou, X.M., Griffin, W.L. 1996.** A xenolith-derived geotherm and the crust–mantle boundary at Qilin, southeastern China. *Lithos* **38**, 41–62.
- Yielding, G., Walsh, J., Watterson, J. 1992.** The prediction of small-scale faulting in reservoirs. *First Break* **10**, 449–460.

Scientific editing by Brian McConnell